Extending Cylindrical Mathematical Absorber Reflection Suppression To Further Reduce Range Scattering Errors

S.F. Gregson[#*1], A.C. Newell[#2], G.E. Hindman[#3]

[#]*Nearfield Systems Inc.*
19730 Magellan Drive, Torrance, CA 90502, USA
[1]sgregson@nearfield.com
[2]anewell@nearfield.com
[3]ghindman@nearfield.com

[*]*Queen Mary, University of London*
Mile End Road, London E1 4NS, UK

***Abstract*— Recent work in developing a mode orthogonalisation and filtering post processing algorithm for multipath suppression in far-field and planar near-field antenna measurement systems has enabled worthwhile improvements to be obtained from the analogous, but mathematically and computationally distinct, cylindrical analogue. This paper presents an overview of the measurement and novel post-processing algorithm as embodied within the cylindrical mathematical absorber reflection suppression technique as well as comparing and contrasting results obtained from the new post-processing algorithms with previously published data.**

I. Introduction

The Mathematical Absorber Reflection Suppression (MARS) measurement and post-processing technique has been in use in academia and industry since it was first introduced in 2005 for use with spherical near-field antenna test systems [1]. During the past seven years the technique has been under continuous development and refinement leading to its extension for use with cylindrical [2], planar [3], far-field [4], and most recently compact antenna test ranges (CATR) [5]. The purpose of the MARS approach is to reduce the influence of scattered signals on measured far-field antenna patterns. This involves the use of a combination of a specific antenna measurement configuration with a mathematical post processing technique that requires only a minimum amount of information about the antenna under test (AUT), near-field probe, and range geometry. The post-processing is applied during the classical near-field to far-field transformation and is general enough to apply to different types of measurement geometries and to different classes of antennas. It has been shown that the mathematical post processing will be most successful if during the measurement the AUT is offset from the origin of the measurement co-ordinate system by an amount that is larger than the dimension of the antenna, for high gain antennas, and by more than a few wavelengths for electrically small antennas [6, 2, 4]. This offset causes the phase of the scattered signals to vary more rapidly over the measurement surface than would ordinarily be the case which results in the introduction of higher order modes. The offset position of the AUT requires smaller angular data point spacing than would be the case for an equivalent ideally centred measurement and therefore a corresponding increase in test time. Although the underlying principles and physical mechanisms are common to all of the MARS implementations, the differences between the respective range geometries necessitate substantial mathematical and computational variations between the various post-processing algorithms. Two recent innovations within the planar [7] and far-field [8] MARS post processing suggested further improvements in multipath rejection were possible in the cylindrical case. The new cylindrical MARS (C-MARS) processing technique, as presented within this paper, enables for the first time scatter suppression to be effectively applied in each of the two orthogonal axes as well as enabling the use of narrower band pass mode filter functions which present better immunity to spurious scattered signals without spectral leakage degrading the resulting MARS processed patterns.

The following sections present an overview of the C-MARS measurement technique and the existing post-processing algorithm before progressing to provide an overview of the novel aspects of the post processing. The success of the extended, more sophisticated, post-processing algorithm is examined by reprocessing existing multipath contaminated measured data and comparing new results against data already published in the open literature.

II. Overview Of Classical Cylindrical MARS

It is common practice in near-field theory to expand measured fields onto a set of orthogonal vector wave functions (*i.e.* "modes") where these modes constitute exact elementary solutions of Maxwell's equations. When expressed in component from, the two sets of cylindrical mode coefficients (CMC) $B_n^1(\gamma), B_n^2(\gamma)$ can be obtained from two measured orthogonal tangential near electric field components using (1) and (2) [2, 9]. Once obtained, these mode coefficients are corrected for the spatial filtering

properties of the near-field probe to determine the true AUT transmitting CMCs [9].

$$B_n^1(\gamma) = \frac{-1}{4\pi^2\kappa^3 H_n'^{(1)}(\kappa\rho_0)} \int_{-\infty}^{\infty}\int_{0}^{2\pi}\left[\frac{n\gamma}{\rho_0}E_z(\rho_0,\phi,z) + \kappa^2 E_\phi(\rho_0,\phi,z)\right]e^{-j(n\phi+\gamma z)}d\phi dz \quad (1)$$

$$B_n^2(\gamma) = \frac{k_0}{4\pi^2\kappa^2 H_n^{(1)}(\kappa\rho_0)} \int_{-\infty}^{\infty}\int_{0}^{2\pi}[E_z(\rho_0,\phi,z)]e^{-j(n\phi+\gamma z)}d\phi dz \quad (2)$$

Asymptotic far-field parameters providing pattern, polarisation, gain, *etc.*, information are obtained from a summation of these modes and through the use of the plane wave condition.

$$E_\theta(r\to\infty,\theta,\phi) = 2jk_0\sin\theta\sum_{n=-\infty}^{\infty}(-j)^n B_n^2(\gamma)e^{jn\phi} \quad (3)$$

$$E_\phi(r\to\infty,\theta,\phi) = -2k_0\sin\theta\sum_{n=-\infty}^{\infty}(-j)^n B_n^1(\gamma)e^{jn\phi} \quad (4)$$

Here, far-field pattern data is naturally tabulated on a regular azimuth over elevation co-ordinate system and is resolved onto a commensurate Ludwig II [10], azimuth over elevation polarisation basis. Thus, once the probe corrected electric far-fields have been determined, the AUT can be rigorously translated back to the origin of the measurement co-ordinate system through the application of a differential phase change [2], *i.e.*,

$$\underline{E}_t(r\to\infty,\theta,\phi) = \underline{E}(r\to\infty,\theta,\phi)e^{j\underline{k}_0\cdot\underline{r}} \quad (5)$$

Here, $\underline{r}$ denotes the displacement vector between the centre of the measurement co-ordinate system and the centre of the aperture of the AUT. Crucially, whilst in principle all we have done is to conceptually, *i.e.* mathematically, translate the AUT back to the origin of the measurement co-ordinate system, from the sampling theorem it is clear that this has the corresponding effect of reducing the number and order of CMCs that are required to accurately represent the radiated fields. The reduced set of translated CMCs can be computed simply through the use of an inversion of equations 3 and 4 [2]. Higher order, non AUT related, CMC can be safely filtered out using a band-pass filter function without compromising the integrity of the underlying antenna pattern function. When expressed mathematically the mode filter becomes,

$$B_n^s(\gamma)\big|_{s=1,2} = \begin{cases} B_n^s(\gamma) & n^2+(\gamma r_{t0})^2 \le (k_0 r_{t0})^2 \\ 0 & \text{elsewhere} \end{cases} \quad (6)$$

Here, s denotes the polarisation index of the CMCs and r_{t0} the optimum MRE, rather than the actual MRE as taken from the near-field measurement where $r_t > r_{t0}$. The mode cut-off is based on the fact that antenna related modes above a certain index number are exponentially attenuated and do not contribute to the far-fields. Thus the mode cut off is determined by the physical dimensions of the AUT. The final step in the processing is to reconstruct the filtered far-field antenna pattern from equations 3 and 4.

In reviewing the standard C-MARS post-processing technique, as summarised above, two enhancements are apparent. Firstly, that the brick-wall band-pass CMC filter function could be replaced with an alternative that better matches the filtered function and its derivatives to zero at the boundaries so as to minimise the deleterious effect of spectral leakage, *i.e.* Gibb's phenomena [10]. Secondly, and as has been successfully demonstrated with the planar MARS (P-MARS) post-processing algorithm, it is possible to apply the existing C-MARS algorithm, as embodied within equations 1 – 6 successively in each of the two orthogonal axes. The remainder of this section is devoted to developing these concepts further.

A great deal of information is available in the open literature regards the use of windowing functions for the reduction of leakage in Fourier analysis. Ref 8 employed a computational electromagnetic simulation of a far-field antenna test range to verify the removal of scattered fields from contaminated far-field data. Within this work, a range of windowing functions were examined as alternatives to the Dirichlet [11], *i.e.* rectangular, window that is embodied within equation 6. Of the available alternatives, the cosine squared and Gaussian functions were found to be particularly attractive candidates as they effectively suppressed non-physical high angular frequency ripple (*i.e.* ringing) on the filtered far-field patterns and were comparatively inexpensive to compute. Although that work was primarily concerned with far-field MARS (F-MARS) as the underlying mathematical treatment was based upon the concepts of cylindrical near-field measurements those results are immediately applicable in this area of application. As such, the $\cos^2$ band pass windowing function was chosen in place of the aforementioned Dirichlet window with an effective bandwidth being again specified by the physical dimensions of the AUT [8]. Although the use of windowing functions has become commonplace when working with spherical-MARS (S-MARS), this is the first time these techniques have been applied to the cylindrical case.

As can be seen, from equation 6, the mode filtering technique described above suppresses the effects of scattering principally in the azimuthal axis. This is because these CMCs are derived from the angular axes and are therefore independent from, artefacts that affect the orthogonal, *i.e.* linear, axis. However, scattering artefacts would be expected to affect both axes and those with a component in the vertical elevation axis are essentially unaffected by this processing. Fortunately, it is a comparatively simple matter to repeat this processing once the filtered antenna pattern function has been rotated by 90° about the horizontal (boresight) axis. Thus, by implementing this processing in both horizontal and vertical axes, all of the range scattering effects can be very effectively suppressed [12]. The simplest way to implement this rotation is to change the tabulating co-ordinate system and polarisation basis from an azimuth over elevation co-ordinate system to an elevation over azimuth system [10]. This has the required effect of exchanging the angular and linear axis during the evaluation of equations 3 and 4 and their inverses [2, 3, 12].

III. Experimental Verification

In order that the new measurement and post-processing technique could be verified, an NSI-200V-3x3 combination planar/cylindrical/spherical antenna test system was used to

acquire a 12” (0.305 m) wide by 11.6” (0.295 m) high X-band slotted waveguide planar array antenna. This measurement configuration can be seen presented in Figure 1 below.

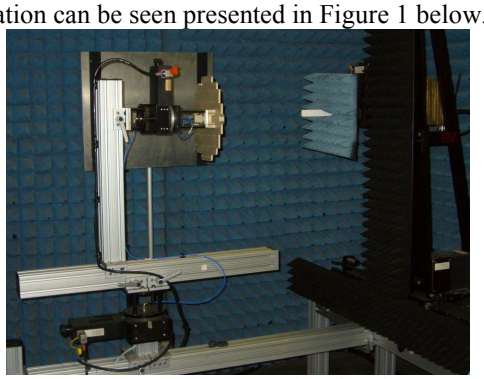

Fig 1 – NSI-200V-3x3 PCS System measuring slotted array antenna in the presence of a reflecting plate.

This system was installed in one of NSI’s small, partially lined anechoic chambers and included a distributed Agilent RF subsystem. A small 0.3 m × 0.3 m removable reflecting plate was installed within the chamber to maximise the scattering and create a “worst case” configuration. Much of the antenna test system itself, *i.e.* the AUT L-bracket and support stand, were not covered in absorber further adding to the general levels of range multipath. A detailed description of the measurement system and previously published results can be found in the open literature, *c.f.* [2]. Figure 2 and 3 present false colour checkerboard plots of the far-field cross-polar and copolar far-field patterns respectively of the linearly polarised planar slotted waveguide array antenna. Here, the electric field was resolved onto a Ludwig II azimuth over elevation polarisation basis. It is clear from inspection of these figures that with the square reflecting panel installed within the chamber, the measurements contain significant levels of range multi-path with a large spectral response being evident in the region $70° \leq Az \leq 80°$, $El = 0°$.

Figures 4 and 5 contain equivalent plots that were obtained using the same cylindrical near-field data set as was plotted in Figures 2 and 3 only here, standard one-axis cylindrical MARS post-processing was employed to filter out most of the artefacts arising from range multi-path. From inspection, it is quite clear that the main specula reflection that was evident at $70° \leq Az \leq 80°$, $El = 0°$ has been almost entirely suppressed. Furthermore, the high angular frequency ripple that was evident in the unfiltered results over much of the far-field is clearly absent in this result, which is very encouraging. Due to the large measurement radius and the comparatively short travel of the linear scan axis, 3’ (0.9 m), these patterns suffer a significant amount of truncation the elevation plane and the pattern data at larger angles is rendered unreliable as a result of the onset of the first order truncation effect [10]. Comparisons were made between the standard and cosine squared windowed one-dimensional C-MARS processing for this data and the difference, as specified by the equivalent multipath level [10], were found to be at an average of -180 dB indicating that this refinement had only a very small effect with this measured data. From inspection of Figures 4 and 5 it is evident that some multipath effects remain and are causing interference fringes to appear that add constructively and destructively as a function of elevation angle only.

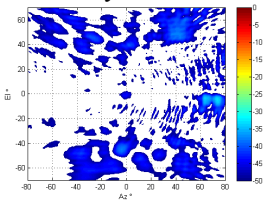

Fig. 2 – Cross-polar pattern of AUT without C-MARS processing.

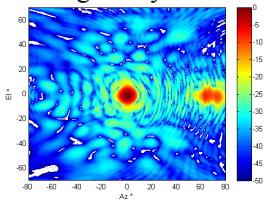

Fig. 3 – Copolar pattern of AUT without C-MARS processing.

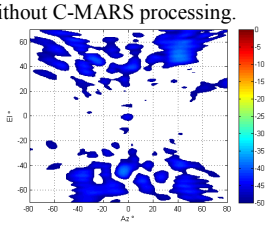

Fig. 4 – Cross-polar pattern of AUT with standard C-MARS processing.

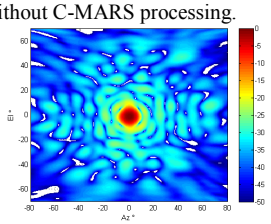

Fig. 5 – Copolar pattern of AUT with standard C-MARS processing.

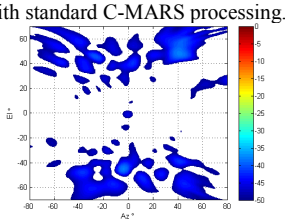

Fig. 6 – Cross-polar pattern of AUT with dual axis C-MARS processing.

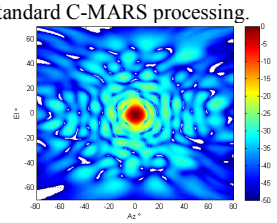

Fig. 7 – Copolar pattern of AUT with dual axis C-MARS processing.

Conversely, Figures 6 and 7 contain equivalent plots that were obtained using the same cylindrical near-field data set as was used in Figure 2 and 3 only this time; the new dual-axis cylindrical MARS process was employed to filter out artefacts arising from range multi-path in both orthogonal axes. Here, it can be seen that the high elevation angular frequency ripple that was previously evident has been reduced. In an effort to try and quantitatively demonstrate the effectiveness of the processing, Figure 8 presents an overlay of four elevation great circle pattern cuts. These far-field pattern cuts were obtained by: standard cylindrical near-field processing with reflecting plate (black trace), standard cylindrical near-field transformation without reflecting plate (blue trace), with reflecting plate and with C-MARS processing (red trace), without reflecting plate but with C-MARS processing (magenta trace). These cuts are shown plotted out to only limited elevation span as the first order truncation effect limits the elevation field of validity to -24° ≤ elevation ≤ 24° which was determined by the height of the AUT, the length of the vertical linear scan, and the AUT-to-probe separation [10]. Here, it is clear that when the reflecting plate was in the chamber the elevation cut was affected by the spurious scattering as evidenced by the difference between the black trace as opposed to the other three traces which were in good agreement with one another. With the application of C-MARS processing the scattering contaminated result (black trace) yields significant improvements with the MARS processed data (red trace) having been brought into very encouraging agreement with the baseline, reference cuts (*i.e.* the blue, or magenta, traces).

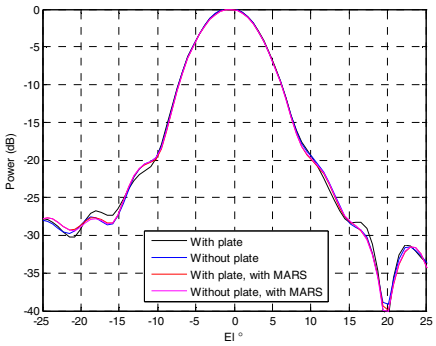

Fig 8 – Comparison of cardinal elevation cuts showing refined C-MARS processing successfully suppressing scattering in the elevation plane.

The amount of scattering in the elevation plane, as introduced by the reflecting plate, is clearly far less pronounced than was the case for the azimuthal plane. This is in part because the AUT is a high gain antenna with comparatively low field strengths illuminating large elevation angles (including the ceiling and the floor), and partly because the action of acquiring the cylindrical near-field data causes the main beam to sequentially illuminate all azimuthal angles including directly illuminating the reflecting plate which leads to the inclusion of a high level specular reflection (which is obvious in the azimuthal great circle cut).

An objective quantitate measure of similarity can be obtained by evaluating the ordinal measure of adjacency between pattern cuts. A detailed description of this comparison technique can be found in the open literature [10]. Here, the correlation coefficient is symmetrical and normalised so that $k = 1$ represents a perfect correlation, whereas $k = 0$ represents no correlation. Three useful comparisons can be made within the angle of validity and these are detailed in Table 1 below. Here, it is clear that the applying MARS has increased the degree of similarity between the pattern cuts as k increased from 0.8333 to 0.8889. When MARS processing was applied to both cuts, the value of k was further increased to 0.9444 indicating that MARS brings the respective pattern cuts into even closer agreement.

1		2		***k*(1,2)**
Plate Present	C-MARS	Plate Present	C-MARS	
Yes	No	No	No	0.8333
Yes	Yes	No	No	0.8889
Yes	Yes	No	Yes	0.9444

Table 1 – Objective quantitative measure of similarity between elevation cuts verifying effectiveness of MARS processing.

The improved rejection of scattering artefacts of the dual-axis C-MARS processing in some part stems from the reduction in the volume of the included region of space. Standard C-MARS removes field originating from a region of space that is exterior to an infinitely long right circular cylinder that is coaxial with the vertical ϕ-axis and that just circumscribes the majority of the current sources. The dual-axis C-MARS processing however, removes field originating outside of a Steinmetz solid which encloses a smaller (finite) volume of space that is formed by the intersection of two right circular cylinders of equal radii that are at right angles to one another.

IV. Summary And Conclusions

As with all forms of MARS processing, Cylindrical MARS processing can be used with a good degree of confidence since all the steps in the measurement and analysis are consistent with the principles of the near-field theory and measurement technique. The offset of the AUT and the resulting smaller data point spacing are valid providing the spacing satisfies the sampling criteria. The translation of the far-field pattern to the origin with a differential phase shift is rigorous. The selection of the mode cut-off for the translated pattern is based on the physical dimensions of the AUT and its translated location. The results of the C-MARS processing will always reduce, but cannot entirely eliminate, the effective of scattering. The final result with C-MARS can be degraded if the sampling of the near-field data is too large, or the mode filter is too small, but this is also true for regular cylindrical processing.

Within this paper, the development and validation of a novel technique to suppress reflections in cylindrical near-field ranges has been reported. The technique is entirely general and can be used to achieve acceptable results with the use of minimal absorber or even with no anechoic chamber.

Finally, as this paper has recounted the preliminary results of an on-going programme of research the planned future work is to include implementing an alternative spherical mode expansion based dual axis post-processing algorithm, *c.f.* [12], to obtain further independent confirmation of these results.

References

[1] G. Hindman, A.C. Newell, “Reflection Suppression in a large spherical near-field range”, AMTA, Newport, RI, Oct. 2005.

[2] S.F. Gregson, A.C. Newell, G.E. Hindman, “Reflection Suppression In Cylindrical Near-Field Antenna Measurement Systems – Cylindrical MARS”, AMTA, Salt Lake City, UT, November 2009.

[3] S.F. Gregson, A.C. Newell, G.E. Hindman, M.J. Carey, "Extension of The Mathematical Absorber Reflection Suppression Technique To The Planar Near-Field Geometry", AMTA, Atlanta, October 2010

[4] S.F. Gregson, B.M. Williams, G.F. Masters, A.C. Newell, G.E. Hindman, "Application of Mathematical Absorber Reflection Suppression To Direct Far-Field Antenna Range Measurements", AMTA, Denver, October 2011.

[5] S.F. Gregson, J. Dupuy, C.G. Parini, A.C. Newell, G.E. Hindman, "Application of Mathematical Absorber Reflection Suppression to Far-Field Antenna Testing", LAPC 2011, Loughborough, November 2011.

[6] G. Hindman, A.C. Newell, “Improving And Extending The Mars Technique To Reduce Scattering Errors”, AMTA, Salt Lake City, UT, November 2009.

[7] S.F. Gregson, A.C. Newell, G.E. Hindman, “Advances In Planar Mathematical Absorber Reflection Suppression”, AMTA, Denver, October 2011.

[8] S.F. Gregson, J. McCormick, B.J. Kerse, A.C. Newell, G.E. Hindman, “Computational and Experimental Verification of Far-Field Mathematical Absorber Reflection Suppression”, the 6th EuCAP, Prague, March 2012.

[9] A.D. Yaghjian, “Near-Field Antenna Measurements On a Cylindrical Surface: A Source Scattering Matrix Formulation”, NBS Technical Note 696, 1977.

[10] S.F. Gregson, J. McCormick, C.G. Parini, “Principles of Planar Near-Field Antenna Measurements”, IET, UK, 2007.

[11] F.J. Harris, “On the Use of Windows for Harmonic Analysis with the Discrete Fourier Transform”, Proc. IEEE Vol. 66, No. 1, pp. 51 – 83, January 1978.

[12] S.F. Gregson, A.C. Newell, G.E. Hindman, “Advances In Planar Mathematical Absorber Reflection Suppression”, AMTA, Denver, October 2011.